Chapter 2

Release currents and concentration profiles

2.1 Introduction

The inositol 1,4,5-trisphosphate receptor channel is found in many different cells (Berridge 1993, Berridge 1997, Berridge et al. 1998). The positive and negative feedback of the cytosolic Ca^{2+} concentration on its open probability induces fascinating spatio-temporal patterns. They have been observed in experiments (Ridgway et al. 1977, Lechleiter et al. 1991a, Nathanson et al. 1994, D'Andrea and Vittur 1995, Marchant et al. 1999, Marchant and Parker 2001, Bootman et al. 1997, Bootman et al. 2001) and have caused a great amount of modeling studies (Falcke 2004, Dupont and Goldbeter 1993, Dupont and Goldbeter 1994, Borghans et al. 1997, De Young and Keizer 1992, Wagner and Keizer 1994, Atri et al. 1993, Sneyd et al. 1993, Sneyd and Sherrat 1997, Sneyd and Dufour 2002, Falcke et al. 1999a, Falcke et al. 1999b, Bär et al. 2000, Falcke et al. 2000a, Falcke 2003b, Falcke 2003a). Although all of them employ the IP_3 receptor as Ca^{2+} source, the properties of release through a single IP_3R or a closely packed group of channels functions has attracted minor attention. In this chapter we will address that question. We will study the Ca^{2+} flux through a single IP_3R and a cluster of release channels. The goal is to elucidate concentration values and concentration gradients that occur at a Ca^{2+} release site. This information serves as a guidance for future modeling of IP_3 mediated Ca^{2+} liberation from the ER. The results do not depend on the specific regulation of the IP_3 receptor by Ca^{2+} and IP_3.

While several studies on the concentration dynamics close to open ryanodine receptor channels exist, little has been done for the IP_3R (Melzer et al. 1984, Melzer

et al. 1987, Blatter et al. 1997, Smith et al. 1998, Izu et al. 2001, Pratusevitch and Balke 1996, Mejia-Alvarez et al. 1999, Rios et al. 1999, Gonzalez et al. 2000) but see (Swillens et al. 1998) for IP_3R . The major differences between release through ryanodine receptor channels and IP_3Rs are the currents and time scales. Currents between 0.35 and 3.3pA are observed in experiments mimicking release from the sarcoplasmic reticulum and elemental events last typically about 10ms (Rios et al. 1999, Mejia-Alvarez et al. 1999). Currents through a single IP_3R are estimated to be in the range from 0.1 to 0.5pA and elemental events last a few hundred milliseconds (Parker et al. 1996a, Sun et al. 1998). Hence, peak concentrations, the spread of free Ca^{2+} in the cytosol and the development of the store content will be different from release by ryanodine receptor channels.

The existing simulations for RyR and analytic calculations demonstrate that huge concentration gradients occur around release sites (Smith et al. 2001). The arrangement of channels in small groups or as single channels on the ER membrane creates spatially discrete release sites (Sun et al. 1998, Marchant and Parker 2001, Mak et al. 2000, Mak and Foskett 1997, Mak and Foskett 1998, Wilson et al. 1998). The typical distance between these release sites is a few micrometers (Marchant and Parker 2001, Thomas et al. 1998) and therefore larger than the diffusion length of free Ca^{2+} in the cytosol of 0.4-1.3µm (Wang and Thompson 1995). Hence, concentration values can differ by 2-3 orders of magnitude between the locations of neighboring channels or channel clusters. Several theoretical studies have shown that the consequences of the discreteness and the concentration gradients can reach from the loss of the ability to oscillate (Thul and Falcke 2004a, Sneyd and Sherrat 1997, Falcke 2003b) to the termination of wave propagation (Sneyd and Sherrat 1997, Falcke et al. 2000b, Coombes 2001). Chapter 2 deals with the loss of the oscillatory regime in more detail. It is therefore important to know the concentration values, gradients and dynamics at the mouth of a releasing channel and at a distance of a few micrometers. The purpose of this study is to provide a quantitative idea of these release characteristics to support further modeling of intracellular Ca^{2+} dynamics. That goal is different from other studies . Whereas they aim at the interpretation and evaluation of specific experiments e.g. by drawing conclusions from dye concentration profiles with respect to the profile of free Ca^{2+}, we try to solve the inverse problem. (Melzer et al. 1984, Melzer et al. 1987, Blatter et al. 1997, Smith et al. 1998, Pratusevitch and Balke 1996, Mejia-Alvarez et al. 1999, Rios et al. 1999, Gonzalez et al. 2000). We focus on establishing the correct relevant parameters and subsequently include the free Ca^{2+} concentration for conditions in vivo. This chapter contains much information which is experimentally relevant as well, especially since we tried to model as close to experimental findings as possible.

We will consider the process of Ca^{2+} release through an open channel. The

dynamics of the channel state (open, closed or inhibited) is not subject of this chapter. Since the channel current through the IP_3R in vivo is not very well known, we will start from lipid bilayer experiments. We transfer the results on the dependence of channel currents on lumenal concentrations to in vivo geometries and concentrations. The following section introduces the model equations and explains the choice of parameter values. The subsequent section will present simulation results. We find that the release currents depend linearly on the bulk concentration of free Ca^{2+} in the lumen but are less sensitive to lumenal buffer concentrations, total lumenal Ca^{2+} content or lumenal diffusion coefficients for ranges of values which can be expected to hold in vivo. The release current is approximately proportional to the square root of the number of open channels in a cluster. Cytosolic concentrations at the location of the cluster range from 25μM to 170μM . Concentration increase due to open clusters in a distance of a few micrometers is found to be in the nanomolar range on the time scale of puff duration. Concentration profiles built up by release decay on a time scale of 0.125-0.250s. Release currents decay bi-exponentially with time scales of less than 1s and a few seconds.

2.2 Methods and parameters

We simulate release of Ca^{2+} in a cylindrical volume divided by the lumenal membrane perpendicular to the cylinder axis. The smaller part represents the ER and the larger part the cytosol. The channel is a pore in the center of the ER membrane with radius R_s (see figure 2.1). The initial condition is the stationary Ca^{2+} - distribution resulting from the pumps and the leak flux P_l. No flux boundary conditions where applied at the outer surface of the cylinder. We chose cylindrical coordinates for our simulations with the positive z-direction pointing from top to bottom in figure2.1.

The model comprises the following species:

- the cytosolic free Ca^{2+} concentration c
- the free Ca^{2+} concentration in the endoplasmic reticulum E
- the concentration of stationary buffer b_s in the cytosol with Ca^{2+} bound
- the concentration of mobile buffer b_m in the cytosol with Ca^{2+} bound
- the concentration of stationary buffer b_{Es} in the endoplasmic reticulum with Ca^{2+} bound

- the concentration of mobile buffer b_{Em} in the endoplasmic reticulum with Ca^{2+} bound.

The reaction-diffusion equations in the cytosol are:

$$\frac{\partial c}{\partial t} = D\nabla^2 c - k_m^+(B_m - b_m)c + k_m^- b_m - k_s^+(B_s - b_s)c + k_s^- b_s$$

$$\frac{\partial b_m}{\partial t} = D_m\nabla^2 b_m + k_m^+(B_m - b_m)c - k_m^- b_m$$

$$\frac{\partial b_s}{\partial t} = k_s^+(B_s - b_s)c - k_s^- b_s.$$

The equations include diffusion of free Ca^{2+} c ($D\nabla^2 c$), diffusion of mobile buffer b_m ($D_m\nabla^2 b_m$) and the reactions of stationary buffer b_s and mobile buffer b_m with free Ca^{2+} ($k_i^+(B_i - b_i)c - k_i^- b_i, i = s, m$). The total concentration of free and mobile buffer $B_i, i = s, m$ is usually homogeneous before the experiments begin. Therefore, the concentration of free buffer, i.e. buffer with no Ca^{2+} bound, can be expressed as $(B_i - b_i), i = s, m$ at any point in space.

In analogy to the equations for the cytosol, the dynamics in the endoplasmic reticulum are:

$$\frac{\partial E}{\partial t} = D_E\nabla^2 E - k_{Em}^+(B_{Em} - b_{Em})E + k_{Em}^- b_{Em} - k_{Es}^+(B_{Es} - b_{Es})E + k_{Es}^- b_{Es}$$

$$\frac{\partial b_{Em}}{\partial t} = D_{Em}\nabla^2 b_{Em} + k_{Em}^+(B_{Em} - b_{Em})E - k_{Em}^- b_{Em}$$

$$\frac{\partial b_{Es}}{\partial t} = k_{Es}^+(B_{Es} - b_{Es})E - k_{Es}^- b_{Es}$$

The flux J through the membrane separating ER and cytosol is given by:

$$J = \Psi\frac{E - \alpha c}{\beta + \gamma E + \delta c}, \qquad r \leq R \tag{2.1}$$

$$J = P_l(E - c) - P_p\frac{c^2}{K_d^2 + c^2}, \qquad r > R \tag{2.2}$$

Here, the values of E and c have to be taken at the membrane (position z_m). R denotes the cluster radius, P_l the coefficient of the leak flux density and P_P the maximal pump strength. The constants in Eq. 2.1 will be determined in the next section. The currents are incorporated into the volume dynamics by setting the boundary condition at the ER membrane like:

$$D\frac{\partial c}{\partial z} = D_E\frac{\partial E}{\partial z} = -J \tag{2.3}$$

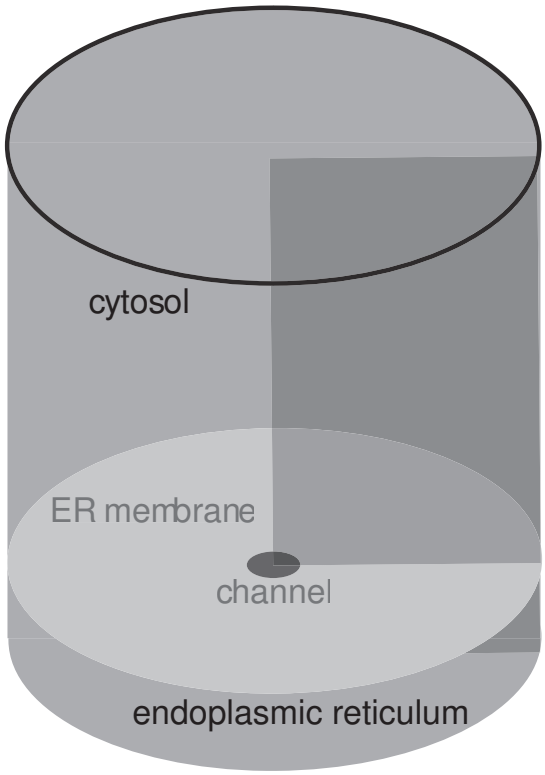

Figure 2.1: Volume within which release was simulated. Rotational symmetry allows to reduce the integration to a plane cutting radially into the volume like shown.

2.2.1 Fitting the single channel flux

The expression for the flux through an open channel (Eq. 2.1) is fitted to data by Bezprozvanny and Ehrlich (Bezprozvanny and Ehrlich 1994). They measured single channel currents of channels reconstituted into planar lipid bilayers. Lipid bilayers are a common tool for studying ion channels (Hille 2001). The bilayer separates two fluid compartments. Some experiments use identical solutions on both sides, but often one sort of ion is present at only one side at the beginning of the experiment. This allows a better controll of feedback mechanisms on the channel dynamics. Originally, the channels sit on small membrane patches obtained from living cells. After putting these pieces into the fluid compartments, they drift to the lipid bilayer and fuse with it. A channel possesses two sides: one heads toward the cytosol, the other toward the lumen. When the channels have reconstituted in the bilayer, one of the compartments corresponds to the cytosol, the other to the lumen. The cytosolic side is termed *cis*, the other *trans*. Bezprozvanny and Ehrlich measured single channel currents with Ba^{2+} as charge

carrier in dependence on the trans concentration. The constants of Eq. 2.1 are fitted by simulation of fluxes in these experiments. In order to perform a fit to the data, we need to mimic the spatial set up of the diffusion problem for a single channel in the lipid bilayer experiment. The current through a single channel is determined - among other parameters - by the geometry of the channel pore. The size of the channel pore is in the range from 10Å^2 (Hille 2001) to 40Å^2 (Lindsay and Williams 1991, Lindsay et al. 1991), if we assume it to be similar to the pore of the ryanodine receptor channel. However, we are interested in concentration profiles on the length scale of a few micrometers. We need to find a compromise in terms of length scales between the geometry of the channel pore and the micrometer length scale in order to reach a computationally treatable model. Here, we use results of Mejía-Alvarez's et al. who performed similar simulations for ryanodine receptor channels (Mejia-Alvarez et al. 1999). They estimated the size of the channel sponge on the lumenal side of the ryanodine receptor channel. The channel sponge is the volume within which negative charges surrounding the channel pore reside. These charges attract the positive Ca^{2+} ions. The radius of this sponge was calculated to be the radius of the Donnan equilibrium potential created by the negative charges (Mejia-Alvarez et al. 1999). It was estimated to be about 5-10nm (Mejia-Alvarez et al. 1999). Therefore, we consider the channel to be a conducting pore in the membrane of approximately this radius. In most simulations we use 6nm (allowing for a numerical grid mesh size of 2nm).

The *trans* chamber in the simulations used to fit the dependence of the current on lumenal concentrations has a radius of 12µm and a thickness of 6.24µm . The *cis* chamber is set up with the same radius and is 5.22µm thick. These measures are sufficient to exclude geometric restrictions, i.e. could serve as a model of a chamber much larger than $(12\mu m)^2\pi \times 5.22\mu m$. The diffusion coefficient for free Ca^{2+} is set to $600\mu m^2 s^{-1}$ corresponding to the value in water (Kushmerick and Podolsky 1969). The *cis* chamber contains 4mM of mobile buffer (k_m^+=$404.67(\mu Ms)^{-1}$, k_m^-=$100s^{-1}$, D_m=$30\mu m^2 s^{-1}$) and 100μM of stationary buffer (k_s^+=$50(\mu Ms)^{-1}$, k_s^-=$100s^{-1}$). However, the buffers have essentially no effect on the current values.

As suggested by the data of Bezprozvanny and Ehrlich (Bezprozvanny and Ehrlich 1994), we take a saturating barrier model of a conducting pore with one ion binding site for the flux (Keener and Sneyd 1998). The general expression of the flux through such a pore is given by Eq. 2.1. Note, that only four of the five constants in this equation are independent. To fit them to the data by Bezprozvanny and Ehrlich we simulate the current I in bilayer experiments. The current is equal to the integral of the flux density over the pore cross section $I = 2F \int_0^{R_s} 2\pi r J dr$ (F Faraday's constant, r radial coordinate, z_m axial coordinate of the membrane, R_s single channel radius). We performed simulations for the homogeneous initial

values $E = 10, 20, 30, 40$mM which were also used in the experiments. In these simulations for the fitting procedure, the expression $J = P_{ch}(E - c)$ was used for the channel flux density. Adjusting P_{ch} for each of the four lumenal Ca^{2+} concentrations in such a way as to reproduce the measured currents allows us to read off the values of the lumenal and cytosolic free Ca^{2+} concentration at the channel and to determine the constants in Eq. 2.1: Ψ=9.3954μms^{-1}, α=1.1497, β=1.1949 10^{-3}, γ=1.1444 $10^{-7}\mu$M $^{-1}$ and δ=1.1556 $10^{-7}\mu$M $^{-1}$.

Local depletion of Ca^{2+} due to the channel flux does not occur in this geometry and with these concentration values and diffusion coefficients. That can be concluded from the values of E at the channel E=9.5, 19.3, 29.2 and 39.2 mM belonging to the initial concentrations $10, 20, 30, 40$mM. Hence, the concentration at the channel is well approximated by concentration values in the bulk of the chamber far away from the channel in lipid bilayer experiments. We will see below that this does not apply to in vivo situations. The results for the constants of Eq. 2.1 imply a half maximum value (β/γ) of 10.44mM for E, which is close to the value of 9mM given in (Bezprozvanny and Ehrlich 1994). The difference $E - \alpha c$ remained large in this lipid bilayer simulations. Hence, there is little effect of Ca^{2+} on the *cis* (cytosolic) side on channel flux density in the lipid bilayer experiments. We will see below, that the concentration values on the lumenal and cytosolic side can be close to each other and the feedback by cytosolic Ca^{2+} becomes relevant in different geometries and for different concentrations in the lumenal part.

2.2.2 Other parameter values

According to (Alberts et al. 1994), p.580, the lumenal space of a flattened cistern of the endoplasmic reticulum of a liver cell is 20-30nm wide. The diameter of tubes belonging to the network part of the ER is up to 60nm. We will consider the case of release from cisternae with a thickness of 28nm and tubular networks. Tubular networks are not described by implementing their real geometry in the simulations. We still use the same cylindrical geometry. However, diffusional transport is reduced due to the tubular shape of the network compared to unobstructed volume and we have to incorporate this reduction. Here, we take advantage of results by Ölveczky and Verkman, who showed that the turtuosity of such a tubular network can be accounted for by reducing the diffusion coefficient by 40-60% (Ölveczky and Verkman 1998). Hence, we model tubular networks by a disc with a height of 60nm and a reduction of lumenal diffusion coefficients to one half of the values for cisternae.

The endogenous cytosolic buffer capacity (B_s/K_s) of immobile buffer was chosen

to be approximately 40 according to findings by Zhou and Neher (1993) . In agreement with the same experiments, that buffer has a rather large dissociation constant of 2μM .

The diffusion coefficient of free Ca^{2+} in the cytosol was measured by Allbritton et al. as $223\mu m^2 s^{-1}$ (Allbritton et al. 1992). The diffusion coefficient of Ca^{2+} in water is approximately $600\mu m^2 s^{-1}$ (Kushmerick and Podolsky 1969). It was found, that the diffusion coefficients of substances in the cytosol, which are believed not to be bound in the cytosol, are approximately one half of the value in water (Kushmerick and Podolsky 1969). This observation supports the value measured by Allbritton et al. and hence we adopt that value as the diffusion coefficient of free Ca^{2+} in the cytosol. It is difficult to estimate the diffusion coefficient of free Ca^{2+} in the ER. In most of the simulations, we use the same value as in the cytosol. However, one could assume that similar to the reduction of diffusion when going from water to the cytosol by one half, a further reduction occurs when going from the cytosol to the lumen of the endoplasmic reticulum. Hence, we will show results with diffusion coefficients of free Ca^{2+} in the ER reduced by one half with respect to value in the cytosol, too.

The results of the measurements of the total Ca^{2+} content of the ER depend on the method used. Direct determination by electron microscopy techniques finds a range of 5-50mM. The highest values occur in the terminal cisternae of the sarcoplasmic reticulum (Meldolesi and Pozzan 1998). Indirect measurements based on fluorescent indicators in the cytosol find 5-10mM (Meldolesi and Pozzan 1998).

Most of the lumenal Ca^{2+} is bound to buffer. The buffer protein calsequestrin is predominantly found in muscle cells. It binds Ca^{2+} with high capacity ($\approx$ 50 ions per molecule) and a K_d of 1mM (Meldolesi and Pozzan 1998). Calreticulin (CRT) is mostly found in non-muscle cells. It binds 20-50 Ca^{2+} ions with low affinity (K_d=0.3-2.0mM) (Michalak et al. 1992).

The concentration of free Ca^{2+} in the endoplasmic reticulum is especially important since it is the driving force for release. It is typically in the range of a few hundred μM and may reach up to 1mM (Meldolesi and Pozzan 1998). A few examples of specific measurements are: in rat embryo R6 fibroblasts 500μM (Foyouzi-Youssefi et al. 2000), in rat myotubes sarcoplasmic reticulum after 6 days in culture 300μM (Robert et al. 1998), in BHK21 fibroblasts $539\pm92\mu$M (Hofer and Schulz 1996), in HeLa cells 60-400μM (Miyawaki et al. 1997). More values can be found in Meldolesi and Pozzan, 1998.

We translate these findings into parameter values for buffers in the endoplasmic reticulum. We use the total concentration of buffers to control the total Ca^{2+} content of the ER and the buffer dissociation constant to set the concentration

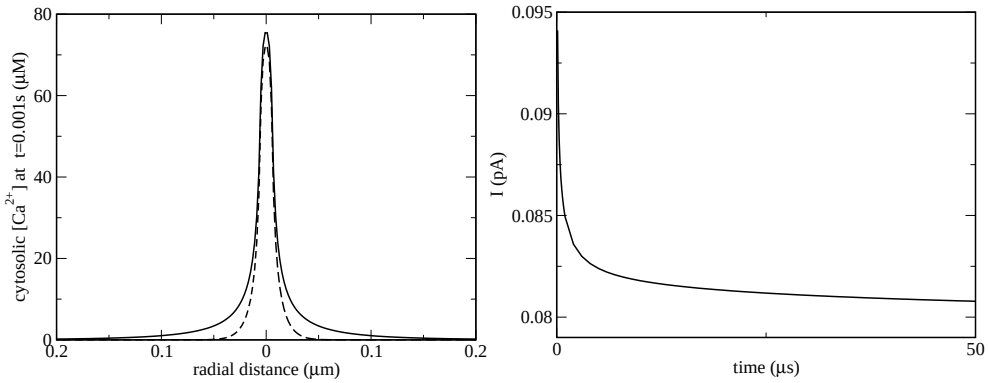

Figure 2.2: Left panel: Spatial profile of free cytosolic Ca^{2+} $0.9\mu s$ (dashed) and $1ms$ (solid) after channel opening. Right panel: Single channel current in the first $50\mu s$ upon channel opening. Parameter values as those of set 2 in Table 2.2 except $k^+_{Em} = k^+_{Es} = 0.2(\mu Ms)^{-1}$.

of free Ca^{2+} . We will show examples with a total content in the range from 5.24mM to 67.87mM and a free concentration from 127μM to 715μM . Similarly, diffusion coefficients of mobile buffers in the lumen of the ER could only be guessed. Consequently, we vary this parameter from 0 to 30$\mu m^2 s^{-1}$.

Numerical simulations use a 4th order Runge Kutta algorithm (Press et al. 2002). Spatial discretization was 2nm for single channel simulations, $2\sqrt{2}$nm and 4nm for larger clusters at the cluster. In a distance r_g of 24 grid points from the boundary of the cluster, we started to increase the spatial grid size continuously like $d_{max}(r-r_g)/[0.25(R-r_g)+(r-r_g)]$ with $d_{max} = 0.3$ and R being the cluster radius. The time discretization is chosen between 25% and 90% of the stability criterion for the smallest spatial step size (Press et al. 2002).

2.3 Results

All results presented in this section are obtained in the cell-like geometry. Thus, the lumenal height is set to 28nm when we refer to cisternae in the ER and 60nm for the tubular ER. Additionally we reduce the diffusion coefficient in the latter case. We begin the presentation with simulation results for single channels. The concentration in a vicinity of a few nanometers of the channel mouth rises within microseconds upon opening of a channel (figure 2.2). On the same time scale of microseconds, the concentration of free lumenal Ca^{2+} at the channel vestibule drops to create the large gradients necessary to transport Ca^{2+} to the channel. All ensuing slow relaxations in this close vicinity of the channel cause

concentration changes typically an order of magnitude smaller than this initial fast rise. This very fast initial time scale appears in the current as well. It quickly drops within the first microseconds to a level which then changes on the time scale of milliseconds.

A channel opens and closes rapidly once it is activated. Typical dwell times are in the range of a few milliseconds (see e.g. (Mak and Foskett 1998, Mak et al. 2001)). The concentrations of fast buffers and free Ca^{2+} within a vicinity of less than 1µm follow or are influenced by this rapid opening and closing of the channel. That is demonstrated in figure 2.3. The concentrations immediately at the channel react with a sharp rise or drop upon channel opening and closing.

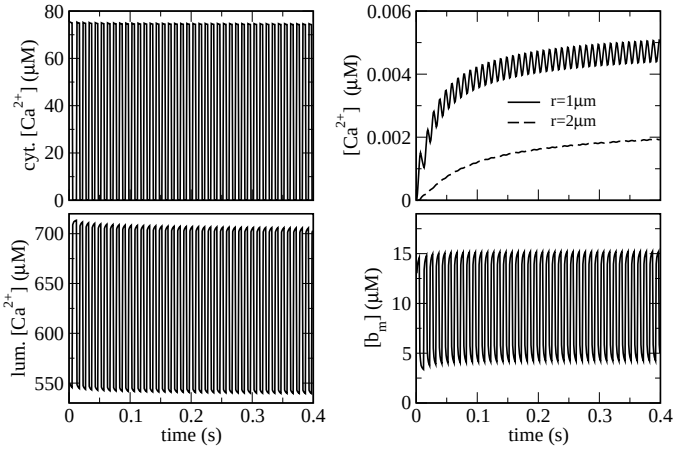

Figure 2.3: Concentration values of cytosolic free Ca^{2+} at the channel mouth (top left) and in a distance of 1µm and 2µm (top right), lumenal free Ca^{2+} at the channel vestibule (bottom left) and cytosolic mobile buffer with Ca^{2+} bound at the channel mouth (bottom right). Open and closed times are 5ms each. For parameter values see Set 2 in Table 2.2. The amplitude of the current pulses is approximately 0.0785pA and decreases by 1% only during the 400ms simulated (data not shown).

Upon closing of the channel, cytosolic free Ca^{2+} drops from approximately 74μM to 93nM within 1ms and to 65nM within the next 4ms (see figure 2.3). These latter values are a factor 3-4 larger than the resting level but negligible compared to the concentration value for an open channel. The cytosolic mobile buffer with Ca^{2+} bound has a resting value of 2.9μM and drops to 3.89μM in between current pulses. The concentration changes of free cytosolic Ca^{2+} due to the rapid opening and closing of the channel are already considerably damped at a distance of 1µm from the channel. In a range of 2µm from the channel, Ca^{2+} rises

monotonically (figure 2.3). Note, that the Ca^{2+} concentrations in the cytosol in figure 2.3 and in all following figures are presented as the increase above resting level. The dynamics of slow buffer shows a smaller amplitude than the fast buffer fluctuations. If we reduce k_m^- from $170s^{-1}$ to $20s^{-1}$ while keeping the value of the dissociation constant K_m, the amplitude of fluctuations of mobile Ca^{2+} -bound buffer drops from 11.45μM to 2.73μM .

When more than one channel in a cluster is activated, the channels open and close on a time scale of a few milliseconds. This leads to an average number of permanently open channels. Therefore we simulate clusters with a given number N_O of open channels. Channels in a cluster are assumed to be closely packed with a distance of 12nm (Swillens et al. 1999). Release through the different channels of a cluster cannot be considered as independent, if the width of the concentration profile formed in the lumen equals approximately or is larger than channel spacing. Our simulations showed that a single channel release current of 0.041pA causes a profile of free Ca^{2+} in the lumen with a full width at half depth of 10nm after 15ms. This width has to be considered as a minimum value, since currents are often larger and release times longer. Hence, the total release current of a cluster is not the sum of the single channel currents of isolated channels, but channels influence each other. That interaction of release through the different channels of a cluster is the reason for the relation between the number of open channels and current we will demonstrate below. Swillens and Dupont found that release through several closely packed individual channels can be very well approximated by release through a single membrane area of corresponding size (Swillens et al. 1999). Based on these observations we model a cluster with several open channels by setting the area of the conducting pore proportional to $N_O R_s^2$ with R_s being the single channel radius. The radius of the pore is then called cluster radius R and is determined by $R = \sqrt{N_O} R_s$. We will simulate release for the typical duration of a puff of 400ms in most of the examples. Section 3.3 will consider longer simulations.

The currents resulting from different numbers of open channels in a cluster for a high filling state of the ER are shown in figure 2.4. They remain essentially constant after an initial relaxation on time scales from a few milliseconds to a few tens of milliseconds for all numbers of open channels. The current increases by about a factor of 10 while going from 1 to 21.77 open channels.

The initial current going through the cluster immediately upon opening is a quadratic function of the cluster radius R. Since spatial profiles of the concentrations have not built up yet, it is proportional to the cluster area. The quadratic dependence quickly turns into an almost linear relationship $I = A_0 + A_1 R$ as the concentration profiles form (figure 2.5). This linear approximation is valid

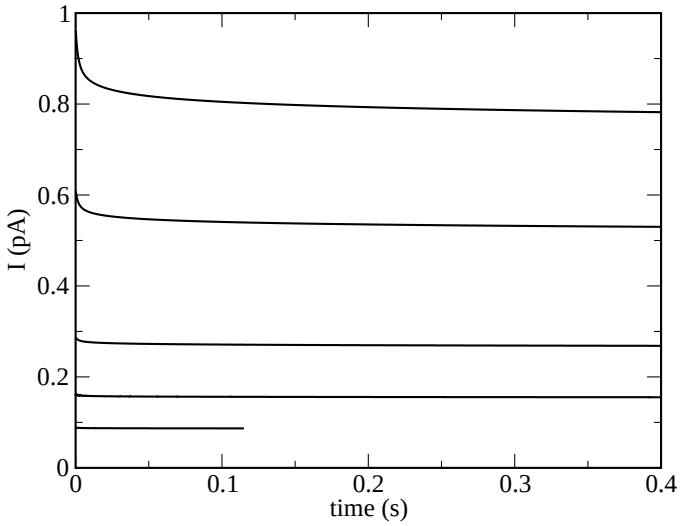

Figure 2.4: Dependence of currents on time. The lines show results for 1, 2, 4, 11.11 and 21.77 open channels from lower to higher values. For parameter values see Set 1 in Table 2.2. Release through a single channel was simulated for 0.115s only.

for a certain range of radii only; e.g. it will not hold for $R \to 0$ because of the constant term A_0. However, it is surprisingly good for radii between 6nm and 50nm. Therefore, currents are proportional to the square root of the number of open channels in that range. The increase of the current with the cluster radius is sublinear for low Ca^{2+} content of the ER (see Fig 2.6).

Concentration values at different distances from the cluster are shown in figure 2.7. Note, that an increase in the number of open channels from 1 to 21.77 entails a rise of the concentration of free cytosolic Ca^{2+} at the location of the cluster from about 100μM to about 170μM only. Hence, the number of open channels and the currents are not very well reflected by the peak concentration values of cytosolic Ca^{2+} (see as well figure 2.9, 2.10, 2.12). This is different for concentrations at a distance of 2.4, 4.8 or 7.2µm from the cluster. They grow faster with increasing current and approximately proportional to the corresponding currents.

The concentration profiles of fast mobile buffer with Ca^{2+} bound (b_m) show essentially the same behavior as the concentration of free cytosolic Ca^{2+} (figure 2.8). The buffer at the cluster saturates for about 10 open channels. The concentration of free cytosolic Ca^{2+} at the cluster with a single open channel would be sufficient to saturate the buffer in a spatially homogeneous system (see figure 2.7). However, the large diffusion flux due to the large gradients prevents saturation. That

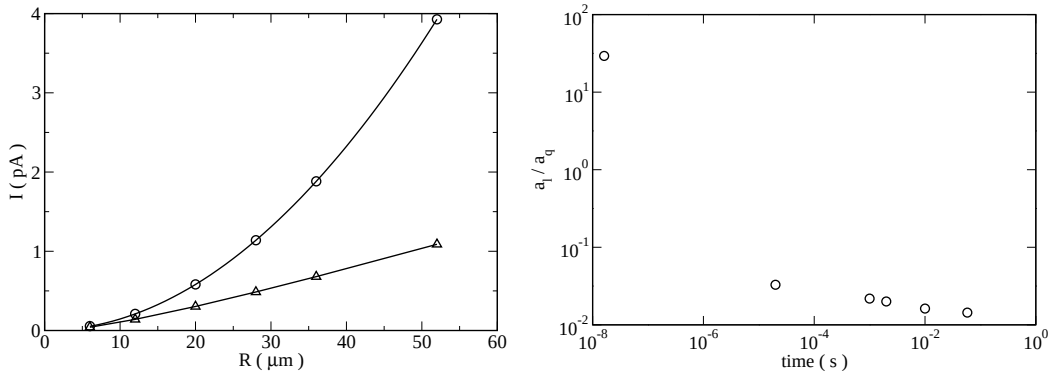

Figure 2.5: Left panel: Current in dependence on cluster radius (◯) R for t=1.4 10^{-8}s and (△) t=0.058s. Right panel: Curves like shown in the left panel were fitted to $I = a_l R + a_q R^2$. Shown is the ratio of the coefficient of the quadratic term to the linear term a_q/a_l in dependence on time. Parameter values are those of Set 1 in Table 2.2 except: E=336.59μM , total concentration of Ca^{2+} in the ER 49.36mM, h_{ER}=5µm . Note that the height of the ER was chosen so as to exclude geometric reasons for the linear dependence of current on R.

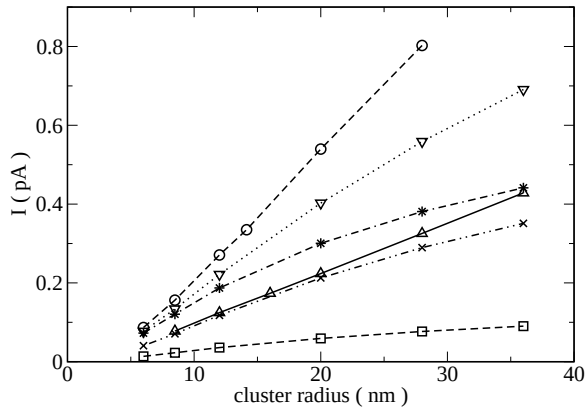

Figure 2.6: Dependence of current on cluster radius at t=0.1s. △ Set 1 except h_{ER}=0.06µm , D_E=23µm^{2}s^{-1} , D_{Em}=3.1µm^{2}s^{-1} , ◯ Set 1, except B_{Es}=100mM, B_{Em}=0, X Set 1 except E=336μM , total lumenal content 5.24mM, B_{Es}=100mM, B_{Em}=0, ▽ Set 1 except total lumenal content 7.43mM, h_{ER}=0.06µm , D_E=110µm^{2}s^{-1} , D_{Em}=16.95µm^{2}s^{-1} , B_{Es}=100mM, B_{Em}=0, □ Set 1 except E=127.8μM , total lumenal content 2.80mM, B_{Es}=100mM, B_{Em}=0, $*$ Set 1 except E=715μM , total lumenal content 7.43mM, B_{Es}=100mM, B_{Em}=0.

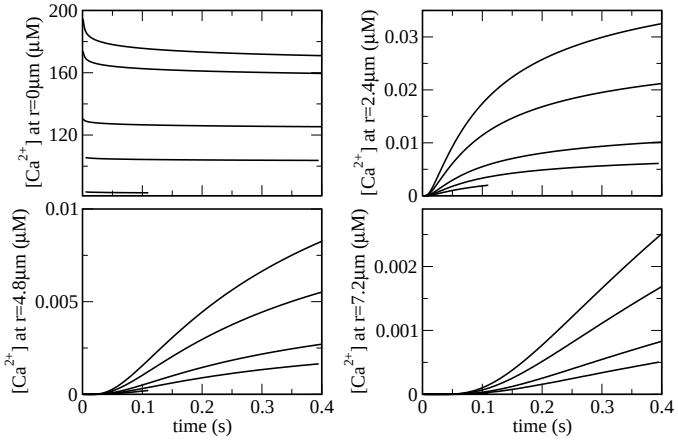

Figure 2.7: Dependence of concentration of cytosolic Ca^{2+} on time at different distances r from the channel cluster. Lines show results for 1, 2, 4, 11.11 and 21.77 open channels from lower to higher values. For parameter values see Set 1 in Table 2.2. Release through a single channel was simulated for 0.115s only.

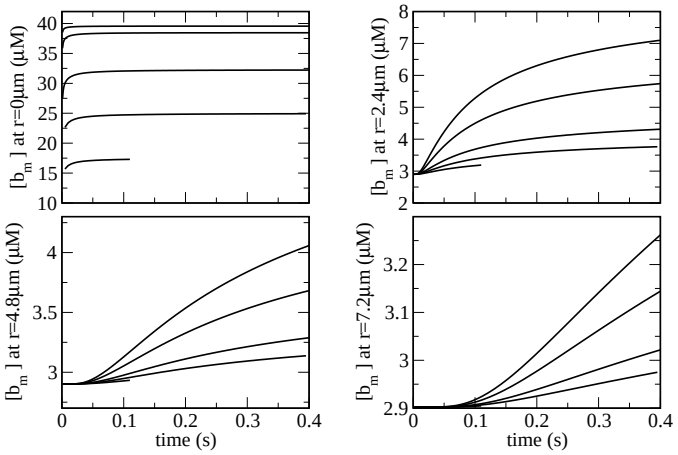

Figure 2.8: Dependence of concentration of cytosolic mobile buffer with Ca^{2+} bound on time belonging to the simulations shown in figure 2.7. The lines show results for 1, 2, 4, 11.11 and 21.77 open channels from lower to higher values. For parameter values see Set 1 in Table 2.2. Release through a single channel was simulated for 0.115s only.

is supported by a comparison with the stationary buffer which already saturates at the cluster with a single open channel (data not shown).

2.3.1 Lumenal parameters

The transport properties of the lumen of the ER like diffusion coefficients or content of mobile buffer are not well known. The local concentrations of free lumenal Ca^{2+} at the cluster suggest that currents are determined by the transport properties since a gradient from the resting level of 715μM far away from the cluster down to approximately 250μM at the cluster builds up (figure 2.9). In order to understand which transport characteristics are crucial, we vary transport parameters. Changing the fraction of mobile buffer from 50% down to stationary buffer only has no major effect on currents and concentrations as figure 2.9 illustrates. Diffusion of free Ca^{2+} alone can compensate for the loss of the transport capacity of mobile buffer, if the diffusion coefficient is in the range of $223\mu m^2 s^{-1}$. Reducing the diffusion coefficient of free Ca^{2+} in the ER to $110\mu m^2 s^{-1}$ in the absence of mobile buffer decreases currents to a negligible degree for small numbers of open channels and by about 50% for large numbers (see Fig 2.9). Since diffusion of free Ca^{2+} is crucial in determining currents, we simulated different transport conditions with the set of parameters representing an ER as a tubular meshwork as well. As mentioned above, it means reducing diffusion by one half and setting the inner height of the ER compartment to 60nm (see figure 2.10). Here, the larger inner height partially compensates for the smaller diffusion coefficient. Note, that decreasing the diffusion coefficient again by almost a factor of 1/2 has less a relative impact than in the cisternae geometry with a lumenal height of 28nm.

Figure 2.11 shows the results for different diffusion coefficients of lumenal free Ca^{2+} . Decreasing the lumenal diffusion coefficient from the cytosolic value of $223\mu m^2 s^{-1}$ down to $23\mu m^2 s^{-1}$ lowers the current by about a factor of 3, but reducing it to $110\mu m^2 s^{-1}$ decreases the current to about 80% of the value with the cytosolic diffusion coefficient only. Hence, if diffusion coefficients in the ER should be one half of the cytosolic diffusion coefficients only (as discussed as a possibility above), that does not have a major impact on the release currents for not too large a number of open channels in a cluster.

The major determinant of currents is the concentration of free Ca^{2+} in the ER. Figure 2.12 shows results for three different concentrations of free lumenal Ca^{2+} . Note, that the current through a single open channel for the lowest concentration is as small as 0.0164pA. The cytosolic concentration of free Ca^{2+} at the location of the channel is about 25μM . Despite the nonlinear dependence of the current

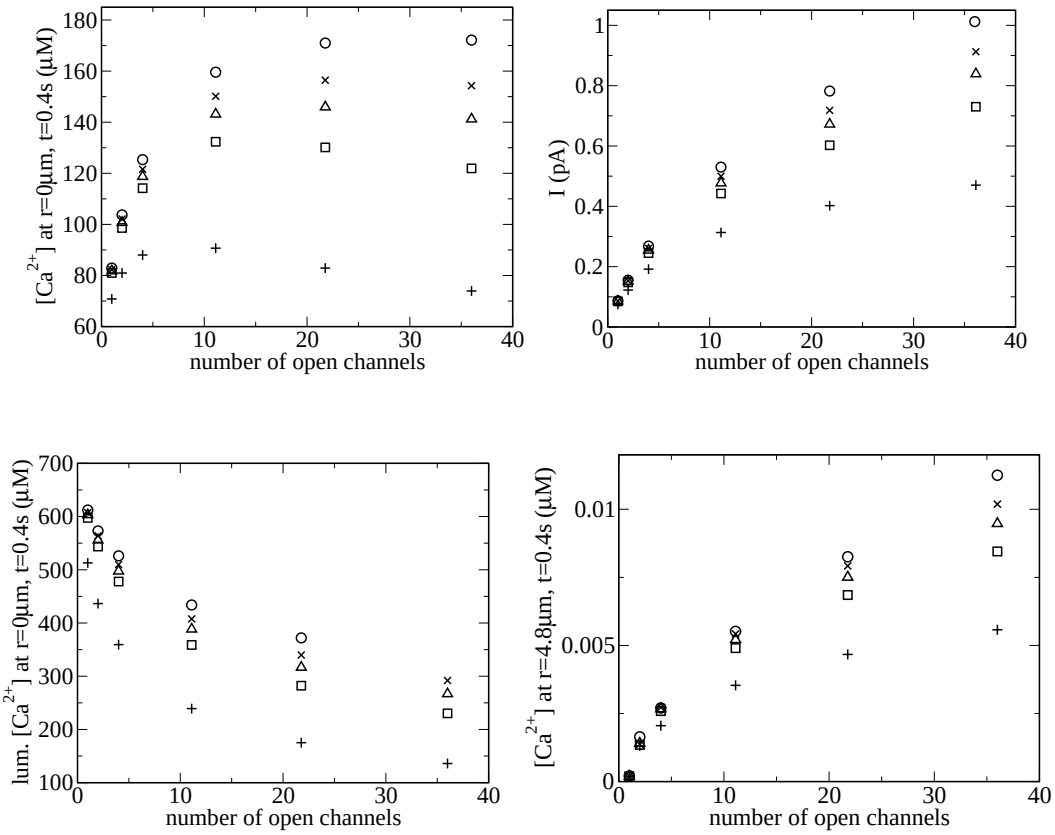

Figure 2.9: Dependence of release on the fraction of lumenal mobile buffer. Top left: Concentration of free cytosolic Ca^{2+} at the cluster in dependence on the number of open channels. Top right: Current values. Bottom left: Concentration of free lumenal Ca^{2+} at the cluster. Bottom right: Concentration of free cytosolic Ca^{2+} in a distance of 4.8µm from the cluster. All panels: Values were taken after the channels were open for 0.4s. In case of a single open channel in the cluster, the values were obtained after 0.115s. For parameter values see Set 1 in Table 2.2 except the concentration of lumenal buffers. They are: B_{Es}=50mM, B_{Em}=50mM ◯, B_{Es}=75mM, B_{Em}=25mM X,B_{Es}=87.5mM, B_{Em}=12.5mM △, B_{Es}=100mM, B_{Em}=0mM □ . The values marked by a + sign were obtained with D_E=110µm^{2}s^{-1} and B_{Es}=100mM, B_{Em}=0mM

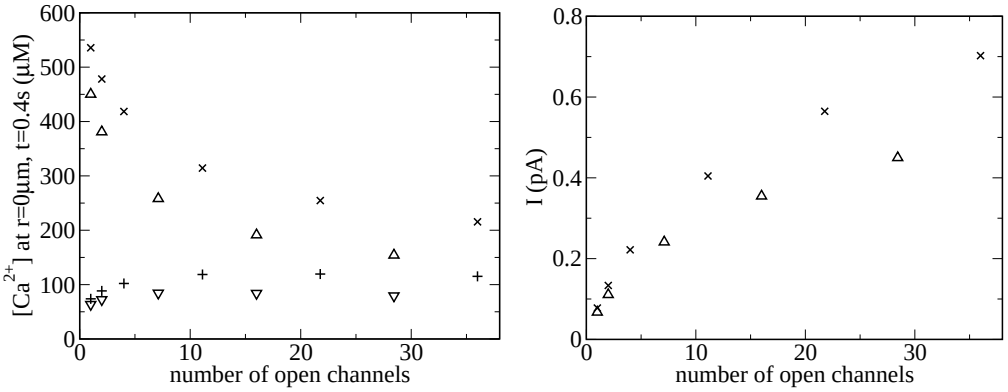

Figure 2.10: Release with parameters mimicking a tubular ER. Left panel: Concentration of free Ca^{2+} at the cluster in dependence on the number of open channels. X and +: Set 2 in Table 2.2, X lumenal concentration, + cytosolic concentration; $\triangle$ and $\triangledown$: Set 2 in Table 2.2 except D_E=63µm^{2}s^{-1} , $D_{Em} = 8.475\mu m^2 s^{-1}$, $\triangle$ lumenal concentration, $\triangledown$ cytosolic concentration. Right panel: Currents for the same parameters as used in the simulations of the left panel. The symbols are chosen accordingly.

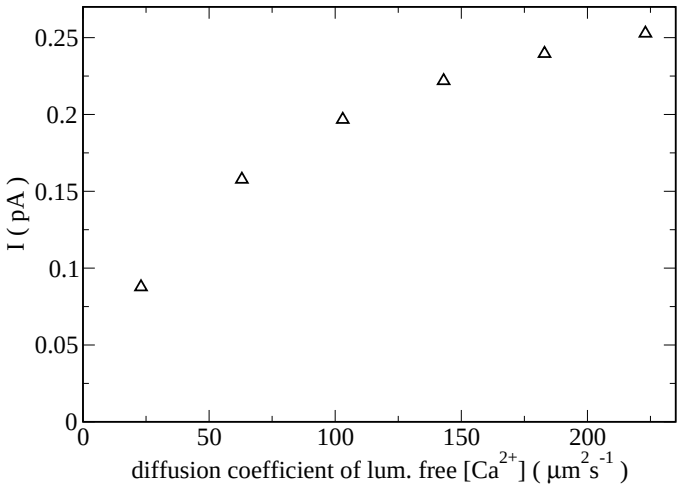

Figure 2.11: Dependence of the release current with 4 open channels at t=0.1s on the diffusion coefficient of lumenal free Ca^{2+} D_E. h_{ER}=0.028µm , concentration of free Ca^{2+} in the ER 715μM , total lumenal concentration 67.87mM, B_{Em}=0, B_{Es}=100mM. For other parameter values see Set 1 of Table 2.2.

density on the lumenal concentration (Eq. 2.1), we find the current to depend linearly on the bulk concentration of free lumenal Ca^{2+} (see figure 2.13). The linear functions approximating the curves in figure 2.13 include a constant term. Hence, the linear dependence will not hold down to E=0. The approximate linearity of the currents in E arises from the almost linear dependence of the total Ca^{2+} content of the cell on E. These findings are in agreement with analytical results for a similar linearized problem in two spatial dimensions (Falcke et al. 2000b) and results by Smith et al. (Smith 1996).

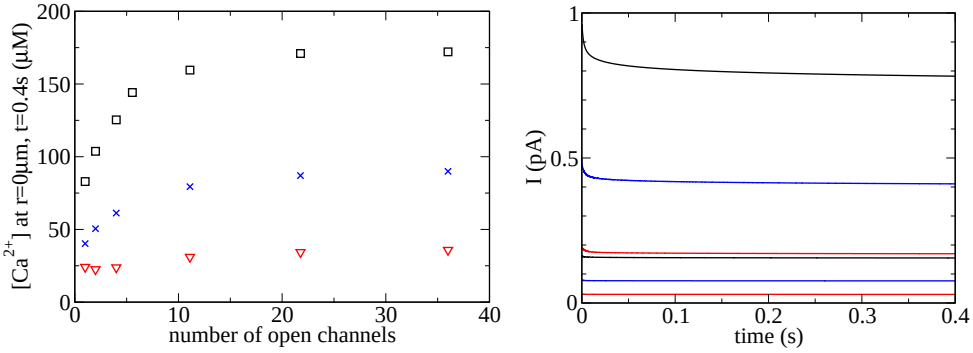

Figure 2.12: Release with different initial concentrations of free lumenal Ca^{2+} . Left panel: Ca^{2+} concentration at the location of the cluster: □ $E = 715.56\mu$M, total concentration of Ca^{2+} in the ER 67.87mM, X $E = 336.59\mu$M, total concentration of Ca^{2+} in the ER 49.36mM, ▽ E=127.80μM , total concentration of Ca^{2+} in the ER 26.87mM. Right panel: Currents for the same sets of parameters as in the right panel and for two different numbers of open channels. Matching colors have same concentration of free and total Ca^{2+} in the ER. For each color: smaller current values 2 open channels, larger values 21.77 open channels. Parameter values not mentioned here are those of Set 1 in Table 2.2.

The total concentration of Ca^{2+} in the ER has little effect on the currents at least for the large radius of the ER disk and the release time of 0.4s we are considering for the time being. Decreasing the total content from about 50mM to about 5mM changes currents at t=0.4s by about 10% only. This is different for smaller radii of the lumenal compartment and longer release times as we will see below.

2.3.2 Cytosolic buffers, spread of released Ca^{2+} in the cytosol

In general, cytosolic concentrations of free Ca^{2+} around a cluster with open channels drop by orders of magnitude on the length of 1µm to 2µm already. That is illustrated by including concentration values at different distances from a cluster

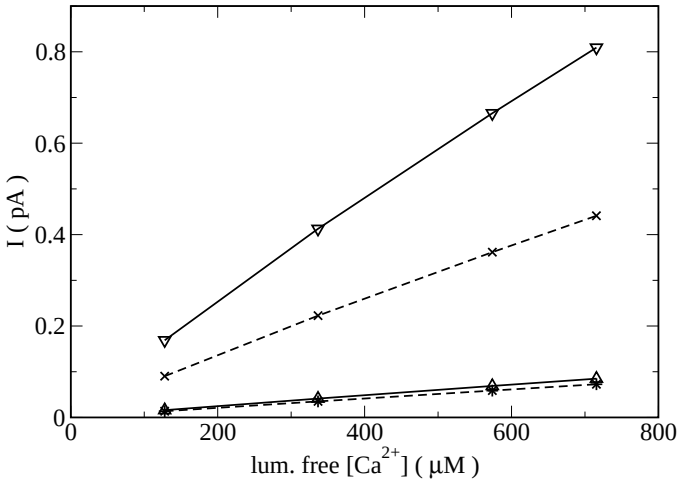

Figure 2.13: Dependence of currents at t=0.1s on the bulk concentration of free lumenal Ca^{2+} . Lumenal buffer concentrations are B_{Es}=100mM, B_{Em}=0 (full lines) and B_{Es}=10mM, B_{Em}=0 (dashed lines). Small current values are obtained with one open channel and large values with 36 open channels.

in figure 2.3, 2.7, 2.9, 2.15. While free Ca^{2+} reaches concentrations of several tens of micromolar at the cluster, concentration increases by a few hundred nanomolar only in a distance of about 1µm (figure 2.15) and by several nanomolar at 2.4µm (figure 2.7, 2.15).

Changing the concentration of mobile buffer in the cytosol from 40μM to 0μM means a change of buffer capacity B_m/K_m by approximately 160. Currents are not influenced in a noticeable degree by such a change and neither by changing the buffer binding rates from fast to slow. Buffers could change currents by affecting the concentration of free Ca^{2+} on the cytosolic side of the cluster (see Eq. 2.1). However, that concentration is rather insensitive to buffer concentrations and properties. Varying buffer binding rates, buffer concentrations, buffer dissociation constants or diffusion of mobile buffer within experimentally reasonable ranges causes changes of the concentration of free cytosolic Ca^{2+} at the cluster of about 1% only.

However, the spread of released Ca^{2+} depends very sensitively on buffer concentrations. Hence, we can only try to determine limiting values of concentrations a few micrometers away from the cluster. We will consider the impact of concentration of fast mobile buffer, buffer binding rates for fixed dissociation constant, variation of dissociation constants of fast buffer and buffer diffusion.

The major effect of increasing buffer binding rates is a stronger localization of the Ca^{2+} profile and larger peak values of the profile of buffer with Ca^{2+} bound (figure 2.14). Furthermore, the rate of rise of concentrations in a fixed distance from

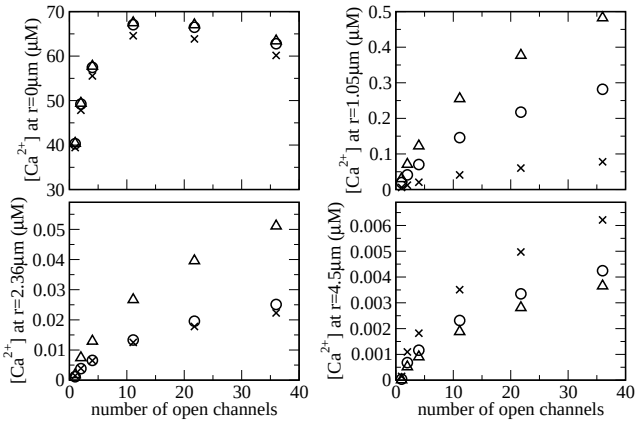

Figure 2.14: Ca^{2+} concentration at different distances from the cluster for different binding rates of mobile buffer. $\triangle$ k_m^+=6.07(μMs)$^{-1}$, $\bigcirc$ k_m^+=20(μMs)$^{-1}$, **X** k_m^+=170(μMs)$^{-1}$, all K_m=0.247μM , D_m=40μm^{2}s^{-1} , B_m=40μM . Note, the fastest buffer (**X**) causes the largest concentration rise at r=4.5μm . The currents at 0.4s belonging to the numbers of open channels for which data are shown are: 0.041pA (at 0.115s), 0.071pA, 0.119pA, 0.218pA, 0.299pA and 0.366pA. Parameter values are those of set 1 in Table 1 except the total concentration of Ca^{2+} in the ER is 49mM resulting in resting concentration of free Ca^{2+} in the ER of 336.7μM, B_{Es}=100mM, B_{Em}=0.

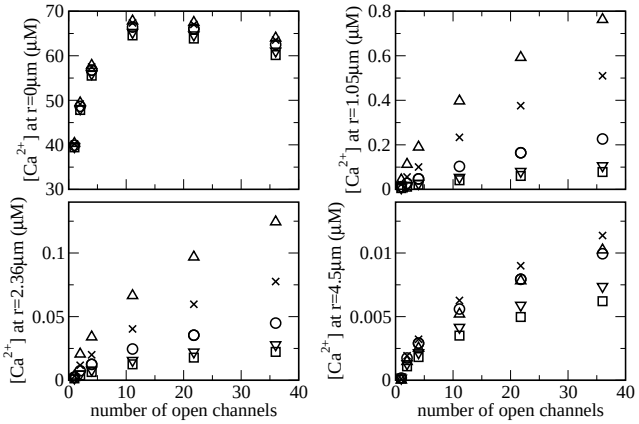

Figure 2.15: Ca^{2+} concentration at different distances from the cluster for different concentrations of mobile buffer. $\triangle$ B_m=0μM , X B_m=5μM , $\bigcirc$ B_m=15μM , $\triangledown$ B_m=30μM , $\square$ B_m=40μM all k_m^+=700(μMs)$^{-1}$, K_m=0.247μM , D_m = 40μm^{2}s^{-1}. The currents at 0.4s belonging to the numbers of open channels for which data are shown are: 0.041pA (at 0.115s), 0.071pA, 0.119pA, 0.218pA, 0.299pA and 0.366pA. For parameter values see Set 1 in Table 2.2 except the total concentration of Ca^{2+} in the ER. It is 49mM resulting in a resting concentration of free Ca^{2+} in the ER of 336.7μM , B_{Es}=100mM, B_{Em}=0.

the cluster strongly depends on buffer rates. Two observations seem remarkable here. First, the increase of diffusional spread while going from k_m^+=81(μMs)$^{-1}$ to k_m^+=25(μMs)$^{-1}$ is comparable to the effect of the much larger step from k_m^+=700(μMs)$^{-1}$ to k_m^+=81(μMs)$^{-1}$. That agrees with results obtained for the stationary profiles, where major changes occurred in that range of binding constants, too (Falcke 2003a). Hence, buffers become slow from that point of view for k^+B smaller than 800s^{-1}. Second, facilitated diffusion of Ca^{2+} by mobile buffer is more effective with fast buffers than with slow ones. It increases the concentration compared to the case without mobile buffer beyond a certain distance from the cluster. However, that increase is in the range of a few nanomolar only.

The results for different concentrations of mobile buffer are shown in figure 2.15. Note, that the increase in free Ca^{2+} concentration at r=4.5μm and t=0.4s without any mobile buffer reaches 11nM only. Rather low concentrations of fast mobile buffer have an impact already. On length scales up to 2.5μm , the use of 5μM fast mobile buffer reduces the spread of free Ca^{2+} considerably. However, buffer assists spread of free Ca^{2+} by facilitated diffusion at $B_m = 5\mu$M and $B_m = 15\mu$M at distances larger than about 4μm . Facilitated diffusion is similar to pickaback. Ca^{2+} binds to mobile buffer and diffuses attached to the buffer through the cytosol. After a while it detaches from the buffer. Hence, the Ca^{2+} concentration at this place is larger than with Ca^{2+} diffusion only. There is essentially no difference between the results for B_m=30μM and B_m=40μM .

The dissociation constant of mobile buffer has a major impact on spatial spread of free Ca^{2+} in areas, where the free Ca^{2+} concentration has approximately the value of the dissociation constant or is smaller than it. Decreasing the dissociation constant reduces the spread of free Ca^{2+} (2.16).

Varying the diffusion constant of mobile buffer D_m from 20μm^{2}s^{-1} to 70μm^{2}s^{-1} reduces the spread of free cytosolic Ca^{2+} on length scales up to 2.5μm (figure 2.17). The faster diffusion of mobile buffer is, the faster Ca^{2+} bound buffer can be exchanged for Ca^{2+} free buffer and the more Ca^{2+} is buffered close to the cluster. However, increasing D_m had little effect on the spread of free cytosolic Ca^{2+} to a distance of 4.5μm . That suggests facilitated diffusion to become important on larger length scales only for large D_m.

It is often easier to measure signal mass in experiments than local rise times or concentrations. The release current can be estimated from signal mass measurements, if the fraction of Ca^{2+} binding to mobile buffer is known. The fraction of released Ca^{2+} binding to mobile buffer does essentially not depend on the current but on the buffer concentration. It increases from about 0.2 to about 0.7 when the buffer concentration is raised from 5μM to 40μM . This is due to the increase

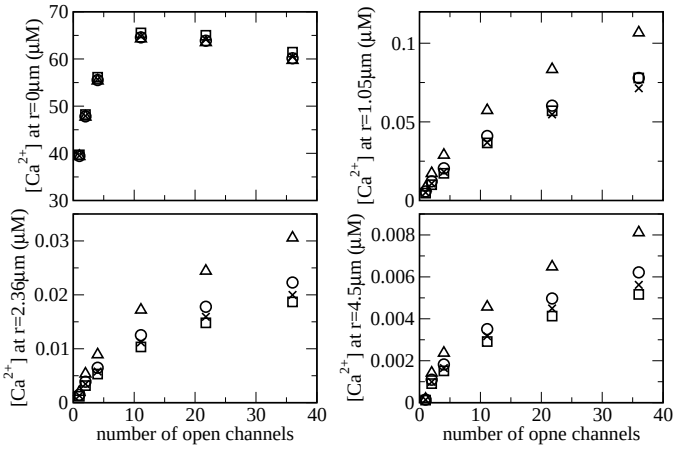

Figure 2.16: Ca^{2+} concentration at different distances from the cluster for different dissociation constants of mobile buffer. $\triangle$ K_m=0.494μM , $\bigcirc$ K_m = 0.247μM, **X** K_m=0.170μM , $\square$ K_m=0.075μM , all k_m^+=700(μMs)$^{-1}$, D_m=40μm^{2}s^{-1} , B_m=40μM . The currents at 0.4s belonging to the numbers of open channels for which data are shown are: 0.041pA (at 0.115s), 0.071pA, 0.119pA, 0.218pA, 0.299pA and 0.366pA. Parameter values are those of set 1 in Table 1 except the total concentration of Ca^{2+} in the ER is 49mM resulting in resting concentration of free Ca^{2+} in the ER of 336.7μM , B_{Es}=100mM, B_{Em}=0.

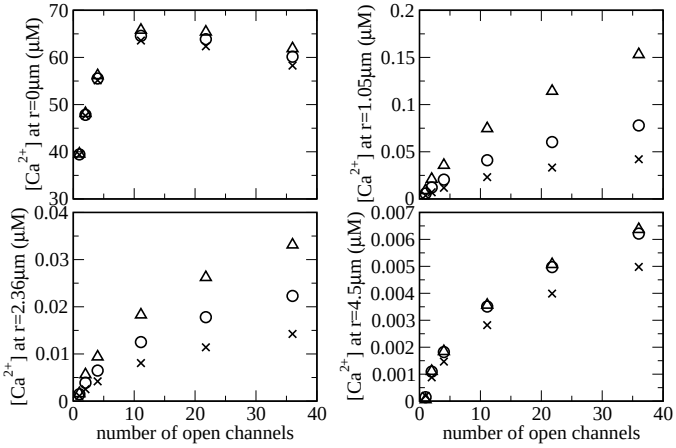

Figure 2.17: Ca^{2+} concentration at different distances from the cluster for different diffusion constants of mobile buffer. $\triangle$ D_m=20μm^{2}s^{-1} , $\bigcirc$ D_m=40μm^{2}s^{-1} , **X** D_m=70μm^{2}s^{-1} , all k_m^+=700(μMs)$^{-1}$, K_m=0.247μM , B_m=40μM . The currents at 0.4s belonging to the numbers of open channels for which data are shown are: 0.041pA (at 0.115s), 0.071pA, 0.119pA, 0.218pA, 0.299pA and 0.366pA. Parameter values are those of set 1 in Table 1 except the total concentration of Ca^{2+} in the ER is 49mM resulting in resting concentration of free Ca^{2+} in the ER of 336.7μM, B_{Es}=100mM, B_{Em}=0.

of volume with high Ca^{2+} concentration with increasing currents.

Species	N_O	A_0 μM	A_1 μM	λ_1 s	A_2 μM	λ_2 s	A_3 μM	λ_3 s
c	4	0.00019	0.267	0.00245	0.207	0.0125	0.0133	0.124
c	36	0.00267	1.876	0.00275	0.544	0.0144	0.0485	0.127
B_m	4	3.016	20.60	0.00210	6.386	0.0182	1.566	0.142
B_m	36	3.332	18.514	0.00346	17.787	0.0234	4.838	0.157
c, r=2.5µm	36	0.0215	0.00676	0.2049	0.00398	0.306	-	-
B_m, r=2.5µm	36	3.272	3.0204	0.0708	2.174	0.245	-	-

Table 2.1: Time scales of the decay of free cytosolic Ca^{2+} c and mobile buffer b_m (see figure 2.18). The decay was fit to $c(t) = A_0 + \sum_i^3 A_i e^{-t/\lambda_i}$. The fit starts 2ms after closure of the cluster. The largest part of the profile peak is dissipated within these 2ms. The concentrations in a distance of 2.5µm from the cluster could be well fit to two exponentials and a constant. N_O is the number of open channels.

It was hypothesized by Parker et al. that the built up of pacemaker Ca^{2+} has a role in wave initiation during long period wave nucleation in Xenopus oocytes. Pace maker Ca^{2+} results from an incomplete decay of the concentration increase due to the previous puff at the time when another puff occurs. In order to obtain an estimate of the decay of cytosolic free Ca^{2+} upon closing of the last open channel in a cluster we simulated this event (see figure 2.18, Table 2.1). Cytosolic concentrations decay on time scales of a few tens of milliseconds at the cluster and a few hundreds of milliseconds in a distance of about 2.5µm away from the cluster (see Table 2.1).

2.3.3 Long time scales, higher cluster density

In the previous sections, we considered release for 0.4s and a single cluster on an ER compartment with a radius of 12µm . That setting applies to isolated clusters or puffs. Release persists for much longer times during waves or oscillations and occurs not through a single cluster but many neighbored clusters simultaneously. We can account for this by the choice of the radius of the cylinder modeling cytosol and ER shown in figure 2.1 or the radius of the lumenal compartment only. That radius determines the volume a single cluster can draw Ca^{2+} from. That volume is determined by the cluster spacing in an array of clusters. Hence, decreasing the radius of the cylinder mimics a larger density of open clusters. The

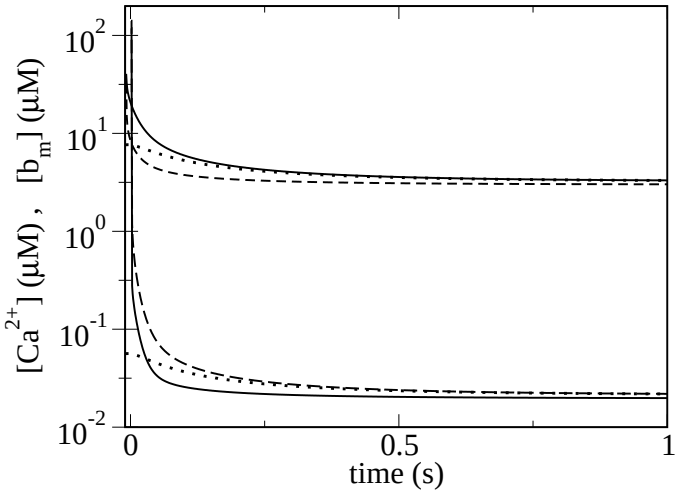

Figure 2.18: Simulation of the decay of cytosolic free Ca^{2+} c and mobile buffer with Ca^{2+} bound b_m upon termination of release after the cluster was open for 0.4s . Note, the logarithmic scale for the concentrations. Bottom group of lines c, top group of lines b_m. Full lines: 4 channels open, concentration at the cluster, dashed lines: 36 channels open, concentration at the cluster, dotted lines: 36 channels open, concentration 4.8μm away from the cluster.

distance of open clusters corresponds to twice the cylinder radius in that picture. Accordingly, the radii 1μm and 2μm used in the simulations conform to cluster distances of 2μm and 4 μm , respectively. With these values, large currents decrease during release lasting a few seconds even with high total concentration of lumenal Ca^{2+} . At the same time, the concentration rise of free cytosolic Ca^{2+} in a distance of 4.5μm in the direction normal to the ER surface reaches values from a few tens of nanomolar to hundreds of nanomolar.

The decay of currents within a few seconds raises the question for the time scales of this process. We simulated release for 10s for two different ER radii and two different concentrations of total Ca^{2+} in the lumen. The experiments which can serve for comparison are superfusion experiments by Marchant and Taylor (1998). The superfusion medium is replaced every 80ms. In order to be compatible with these experiments - at least as far as parameter values are known and our modeling frame work allows - we set cytosolic concentration values to resting level every 80ms and collect the amount released in 80ms time bins. The results can be fitted very well to a sum of two exponentials and a constant. We adopt this representation to be compatible with experimental results. The relative amplitudes of the exponentials and time scales are shown in Figs. 2.19, 2.20.

Half times and relative amplitudes are in the range observed experimentally in hepatocytes (Marchant and Taylor 1998, Dufour et al. 1997). The half times

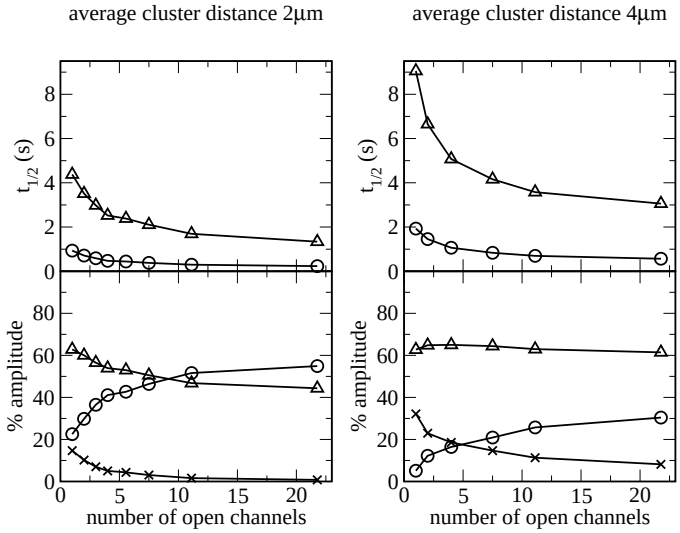

Figure 2.19: Analysis of the temporal decay of release from the ER with high initial lumenal content. Amounts released within 80ms were sampled in bins. The result was fitted to $A_0+A_1e^{(t\ln 2)/t^1_{1/2}}+A_2e^{(t\ln 2)/t^2_{1/2}}$. The symbols of the amplitude curves match the symbols of the corresponding $t_{1/2}$. X marks the contribution of the constant term. Left hand side: Radius of the lumenal compartment is 1µm corresponding to an average cluster distance of 2µm . Right hand side: Radius of the lumenal compartment is 2µm corresponding to an average cluster distance of 4µm . The upper row shows the $t_{1/2}$, the lower row the relative amplitude. Initial concentration of free lumenal Ca^{2+} E=715.56μM , initial total concentration of Ca^{2+} in the ER 67.87mM, P_p=P_l=0.

decrease with increasing number of open channels, increasing cluster density and with decreasing lumenal content. The same qualitative behavior holds for the fraction of the amplitude of the exponential with the smaller half time. The ER with lower content can maintain release at numbers of open channels presumably typical for oscillations for about 4s at low cluster density and about 2s for high cluster density (estimated by twice the longer $t_{1/2}$). The ER with high content can maintain release 2 to 3 times longer. Hence, depletion of the ER may occur during Ca^{2+} oscillations with release phases of several seconds for low and intermediate lumenal content.

2.4 Discussion

The first step of the study we have presented here is a fit of a simple single binding site pore expression for the channel current to data by Bezprozvanny et al.

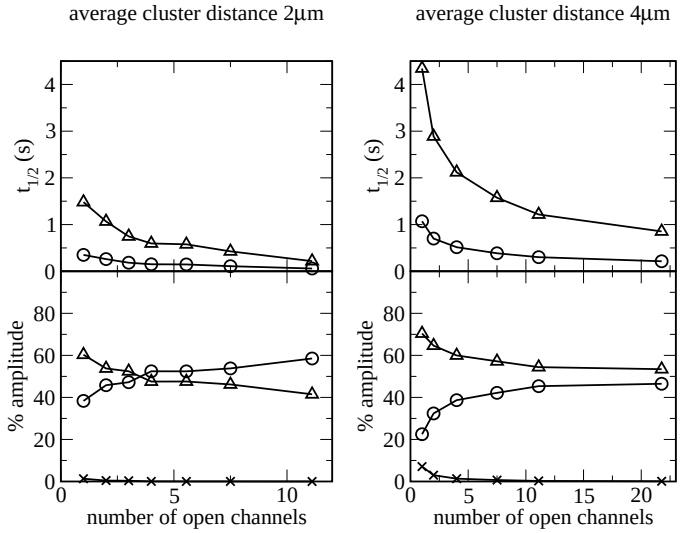

Figure 2.20: Analysis of the temporal decay of release from the ER with low initial lumenal content. Amounts released within 80ms were sampled in bins. The result was fitted to $A_0 + A_1 e^{(t \ln 2)/t^1_{1/2}} + A_2 e^{(t \ln 2)/t^2_{1/2}}$. The symbols of the amplitude curves match the symbols of the corresponding $t_{1/2}$. X marks the contribution of the constant term. Left hand side: Radius of the lumenal compartment is 1µm corresponding to an average cluster distance of 2µm . Right hand side: Radius of the lumenal compartment is 2µm corresponding to an average cluster distance of 4µm . The upper row shows the $t_{1/2}$, the lower row the relative amplitude. Initial concentration of free lumenal Ca^{2+} E=336.6μM , initial total concentration of Ca^{2+} in the ER 5.24mM, P_p=P_l=0.

(Bezprozvanny and Ehrlich 1994). Our fit leads to a similar half maximum value for the dependence of current on lumenal Ca^{2+} and confirms, that the feedback of cytosolic Ca^{2+} on the current is negligible in the lipid bilayer experiments. However, with concentrations occurring in the ER and cytosol of a cell, this feedback becomes important. The constants obtained in this fit should apply to all IP_3R subtypes since their conduction properties are similar (Taylor 1998). The scaling of Ψ with the cross section of the single channel conducting pore has to be observed when Eq. 2.1 is used in other models.

We find that large gradients build up in the lumen during release which are necessary to transport Ca^{2+} to the channel. Thus transport properties of the ER were expected to be a major factor in determining the release current. However, release currents change by about 30% only within a realistic range of diffusion coefficients of free Ca^{2+} in the ER. They were neither very sensitive to the fraction of mobile buffer.

The proportionality of the release current to $N_O^{\frac{1}{m}}$ with $m \geq 2$ is important for

interpreting experiments of the IP_3 dependence of release currents. As an example we consider results by Parker et al. (Parker et al. 1996b) on the increase of the initial release rate with IP_3 in local measurements. The initial rate rises like $120(\mu Ms)^{-1}$ $[IP_3]/([IP_3] + 600nM)$. With the above proportionality, we can deduce from this expression how many IP_3 molecules need to bind to an IP_3 receptor for channel opening. Because the initial rate equals the current, the rate scales as $\sqrt{N_O}$. Hence, the number of open channels is proportional to $([IP_3]/([IP_3] + K_{IP_3}))^2$. If we assume that IP_3 binds in a noncooperative way, this dependence on the IP_3 concentration entails that two IP_3 molecules bind to the receptor. Note that our results cannot be directly transferred to global measurements since global release might increase by opening of channels situated not close to an open channel. Then, the spatial proximity which is a prerequisite for the above proportionality does not hold any more.

Currents in our simulations are in the range from 0.015pA (E=127μM , 1 open channel) to 0.8pA (E=715μM , 36 open channels). We can compare this to signal mass released in Xenopus oocytes, since signal mass was found to be the most reliable measurement in characterization of puffs (Sun et al. 1998). According to (Sun et al. 1998), between 0.004pC and 0.22pC are released during puffs (most of them release less than 0.12pC). The amount of Ca^{2+} released in 0.4s in our simulations spans the range from 0.006pC to 0.32pC. Hence, it covers the range measured in Xenopus oocytes. We can compare more specifically the signal mass for 5 open channels and different values of free lumenal concentrations. The number of 5 open channels is typical for a puff (Sun et al. 1998). That is 0.021pC at E=127μM and 0.055pC at E=336μM . Sun et al. assume that one half of the released Ca^{2+} binds to the dye. However, we find that 70% bind to the dye at a dye concentration of 40μM . Hence, most of the puffs reported in (Sun et al. 1998) are actually below 0.0857pC. If we further assume puffs with a large signal mass to last 600ms instead of 400ms (see (Sun et al. 1998)), we need to multiply the simulated values with a factor 1.5. Finally, we find that the range of signal mass in our simulations agrees with the range found for puffs in Xenopus oocytes, if the concentration of free lumenal Ca^{2+} is between 127μM and 336μM . That is in agreement with recent measurements of free lumenal Ca^{2+} in Xenopus oocytes (Falcke et al. 2003).

The increase of cytosolic Ca^{2+} in a distance of 4.5μm from an open channel after 0.4s of release is rather small. It stays below 15nM in the examples we have presented. If the resting concentration is 100nM (40nM) and three Ca^{2+} ions need to bind in order for the channel to open, then a rise of 15nM increases the opening probability per unit time by a factor of $(115/100)^3 = 1.52$ at 100nM and $(55/40)^3 = 2.6$ at 40nM base level, respectively. According to recent measurements, a resting level of 100nM appears more realistic in Xenopus oocyte (Falcke

et al. 2003). The rather small increase in the open probability caused by releasing clusters in the vicinity of a closed cluster coincides with the finding that a single puff cannot initiate a wave (Marchant and Parker 2001). If there are three releasing clusters in the vicinity of a closed cluster, the open probability already increases by a factor of 3.05 (resting level 100nM).

The time scale of the decay of concentration profiles upon the termination of release can be set in relation to puff frequencies just below the wave initiation threshold (Marchant et al. 1999). Marchant et al. measured the distribution of time intervals between puffs in a group of clusters. The distribution has a peak for 1.5s-2s and falls to half the peak value in the time bin 0-0.5s (Marchant et al. 1999). Hence, only very few puffs show a frequency of more than $2s^{-1}$. An impact of local pacemaker Ca^{2+} on puff behavior would require that the IP_3Rs are able to sense concentration differences in the nM range. Moreover, puff frequencies need to be about $3s^{-1}$ (table 2.1), because otherwise, the decay of the concentration profile has already proceeded to far to show any influence. These considerations apply, if diffusion dissipates release profiles completely. Pacemaker Ca^{2+} can of course still occur as global concentration increase in which case its dynamics is determined by other processes than diffusion.

We found facilitated diffusion as a factor increasing cytosolic free Ca^{2+} far away from the cluster in several simulations. Our results indicate the existence of a critical distance above which facilitated diffusion increases lumenal free Ca^{2+} compared to the case without mobile cytosolic buffer. That radius increases with time and depends on buffer and release parameters. At the parameters of fast buffers used in our simulation (B_m, K_m), facilitated diffusion increased cytosolic Ca^{2+} beyond 3.9-5.5μm at t=0.4s by typically 1-2nM.

Buffers had essentially no effect on the peak concentration values of free cytosolic Ca^{2+} at the channel cluster in our simulations. This is important in assessing experiments using buffers to eliminate feedback of Ca^{2+} on the channel dynamics. Typically, high concentrations of EGTA are used. The full width at half maximum is 10.7nm only with 2mM buffer concentration in our simulations. However, the half maximum is still a concentration of a few tens of micromolar of free Ca^{2+} typically, which is capable of exerting a feedback on channel behavior.

Most simplified models up to date couple regulation of the channel to the average bulk concentration. However, the concentration experienced by the regulatory binding sites of the IP_3R is 2-3 orders of magnitude larger than the average bulk concentration. Most models of channel dynamics assume dissociation constants for binding of Ca^{2+} to the activating binding site in the submicromolar range. Furthermore, lipid bilayer experiments using cations different from Ca^{2+} as the ion conducted by the IP_3R - hence allowing for separate control of the Ca^{2+}

concentration on the *cis* side - indicate that these dissociation constants are realistic indeed (Ramos-Franco et al. 1998, Mak et al. 1998, Mak et al. 1999, Mak et al. 2001). Additionally, if channels are able to sense an open cluster 2-5μm away or pacemaker Ca^{2+} , they need to be able to sense concentration changes in the nanomolar range. These findings and considerations entail a very high opening probability for all IP_3 -bound channels of a cluster as soon as the first channel of a cluster opens, since the dissociation constant of the activating Ca^{2+} binding site is much smaller than the concentrations at the cluster location. Together with the large spatial gradients occurring around an open cluster, that will have consequences for the existence and stability of asymptotic solutions of deterministic cluster models. We will discuss that topic in the next chapter.

The time scales and the amplitudes of the exponential functions describing the decay of currents in simulations over 10s (Figs. 2.19, 2.20) are in the range of but not equal to experimentally determined values (Marchant and Taylor 1998, Dufour et al. 1997). These values are obtained in experiments designed to evaluate time scales of channel dynamics. The smallest $t_{1/2}$ we find are larger than the experimental values when a high lumenal content is used in the simulation but smaller when we apply a low lumenal content (Marchant and Taylor 1998). An analysis based on better knowledge of lumenal parameters would be necessary to assess the meaning of these findings for experimental results. However, conclusions on channel state dynamics cannot be drawn from the mere existence of more than one time scale in current decay as was done in these experimental studies.

The geometry we have chosen for our simulations applies best to cisternae of the ER since it allows for diffusion into half space only. The radius of tubes is assumed to be 30nm (Alberts et al. 1994). The gradient of profiles created by small currents (<0.1pA) decreases by about 80% on this length scale and clusters creating this current have a radius much smaller than the tube radius. Hence, for small clusters, the tube will essentially act like the membrane of a cisterna. The Ca^{2+} gradient created by currents in the range of 0.3pA decreases by about 50% on the first 30nm. Hence, diffusion "around" the tube will have an impact. However, the reduced peak value of cytosolic Ca^{2+} due to diffusion increases the difference $E - \alpha c$ in Eq. 2.1 which increases the current and hence counteracts the decrease of cytosolic Ca^{2+} . Therefore, we assume that our simulations are a good approximation for Ca^{2+} concentration profiles close to a cluster on a tube of the ER as well. The results which will depend on whether cisternae or tubular ER is modelled are the time scales of the decay of currents.

In summary, our results provide information on the relation of currents to the number of open channels and current values to the concentration of free lumenal

Ca^{2+} which assist in the analysis of experimental results. We provide ranges of values for concentrations and concentration gradients on which modeling can be based. Models presented in the following chapters build on these results.

Parameter	Set 1 Value	Set 2 Value	Unit
Geometric parameters:			
height of the cytosol	9		µm
radius of the cytosol	12		µm
height of the ER h_{ER}	0.028	0.060	µm
radius of the ER R_{ER}	12		µm
leak flux coefficient P_l	0.02		µm s^{-1}
channel flux constants:			
Ψ	9.3954		μms^{-1}
α	1.497 10^{-3}		
β	1.1949 10^{-4}		
γ	1.1444 10^{-7}		μM^{-1}
δ	1.1556 10^{-7}		μM^{-1}
single channel radius R_s	0.006		µm
pump flux coefficient P_p	40		μM μms^{-1}
pump diss. coefficient K_d	0.2		µM
diffusion coefficient:			
D	223		μm^2 s^{-1}
D_E	223	110	μm^2 s^{-1}
D_m	40		μm^2 s^{-1}
D_{Em}	30	16.95	μm^2 s^{-1}
on-rates of buffers:			
k_s^+	50		$(\mu Ms)^{-1}$
k_m^+	700		$(\mu Ms)^{-1}$
k_{Em}^+	1		$(\mu Ms)^{-1}$
k_{Es}^+	1		$(\mu Ms)^{-1}$
buffer diss. constants $\frac{k_i^-}{k_i^+}$:			
K_s	2		μM
K_m	0.2428		μM
K_{Es}	350		μM
K_{Em}	350		μM
total concentrations of buffers:			
B_s	80		μM
B_m	40		µM
B_{Es}	50	5	mM
B_{Em}	50	5	mM
total concentration of Ca^{2+} in the ER	67.87	7.430	mM
resting concentration of free Ca^{2+} in the ER	715.56	715.56	μM

Table 2.2: Parameters of simulations. Voids in a "Value" column mean that the value of Set 1 is valid.